LA-UR- 10-00283

Approved for public release; distribution is unlimited.

Title: COLD-START CHARACTERISTICS OF POLYMER ELECTROLYTE FUEL CELLS

Author(s): Y. Wang
J. Mishler
P. P. Mukherjee
R. Mukundan
R. L. Borup

Submitted to: IHTC14-23004: International Heat Transfer Conference

Los Alamos
NATIONAL LABORATORY

The 14th International Heat Transfer Conference (IHTC)
August 7-13, 2010, Washington D.C., USA

IHTC14-23004

COLD-START CHARACTERISTICS OF POLYMER ELECTROLYTE FUEL CELLS

Yun Wang
Renewable Energy Resources Lab (RERL) and
National Fuel Cell Research Center
The University of California, Irvine
Irvine, CA 92697-3975, USA

Jeff Mishler
Renewable Energy Resources Lab (RERL) and
National Fuel Cell Research Center
The University of California, Irvine
Irvine, CA 92697-3975, USA

Partha P. Mukherjee
Oak Ridge National Laboratory,
Oak Ridge, TN 37830-8050

Rangachary Mukundan
Los Alamos National Laboratory,
Los Alamos, NM, 87545, USA

Rodney L. Borup
Los Alamos National Laboratory,
Los Alamos, NM, 87545, USA

ABSTRACT

In this paper, we investigate the electrochemical reaction kinetics, species transport, and solid water dynamics in a polymer electrolyte fuel cell (PEFC) during cold start. A simplified analysis is developed to enable the evaluation of the impact of ice volume fraction on cell performance during cold-start. Supporting neutron imaging data are also provided to reveal the real-time water evolution. Temperature-dependent voltage changes due to the reaction kinetics and ohmic loss are also analyzed based on the ionic conductivity of the membrane at subfreezing temperature. The analysis is valuable for the fundamental study of PEFC cold-start.

INTRODUCTION

Polymer electrolyte fuel cell (PEFC) has been receiving growing interests in new energy development due to its noteworthy features of high efficiency and zero emission. Over decades' development, significant progresses of PEFC technology have been achieved in terms of performance, durability and cost [1]. Startup from a subfreezing condition, also called "cold start", has been one of the technical challenges hindering the automobile application of PEFCs. Under freezing environmental conditions, water produced has a tendency to freeze in open pores in the catalyst layer and GDL, rather than be removed from the fuel cell, thus creating mass transport limitations which eventually end the ability for operation.

Research on PEFC cold start is relatively new [2-13]. Hishinuma et al. [2], Wilson et al. [3], McDonald el al.[4] and Cho et al.[5] conducted early studies on cold start. Hishinuma et al.[2] investigated cold-start down to ~-25°C and found waste heat generated by fuel cell might be sufficient to increase the PEFC temperature to 0 °C. Wilson et al. [3] investigated the impact of the freeze/thaw cycles on the electrode performance and concluded that freezing may not be detrimental to the integrity of the catalyst layer and membrane assembly. McDonald el al. [4] also conducted experiments to investigate the physical change in the electrolyte membrane due to freeze/thaw cycling. Cho et al. [5] carried out a study on cell degradation related to the thermal cycle and concluded that water freezing may be a source of cell degradation. Recently, Oszcipok et al. [6] examined the isothermal potentiostatic cold start and observed that water freezes in the cathode electrode, microporous layer, and the GDL. Yana et al. [7] investigated the impact of sub-freezing temperatures on components and observed delamination of the catalyst layer during cold start. Mukundan et al. examined the fuel cell performance at subfreezing temperature and studied the influence of carbon paper and carbon cloth GDLs [8]. Wang [9] presented a theoretical analysis on PEFC cold start operation and identified three stages of cold start. His following work [10-12] furthered the analysis based on the framework developed by Ref. [9]. In addition to theoretical analysis, Mao and Wang [13], Meng [14], and Jiao and Li [15] proposed multi-dimension cold-start models and examined the distributions of ice within the PEFC fuel cell assembly.

This paper develops a detailed analysis of cold start on the solid water dynamics and temperature-dependent voltage variations. Supporting data from the neutron imaging measurement are provided. Oxygen profiles, overpotential change, temperature dependent voltage changes, and associated analysis are

presented to improve the fundamental understanding of fuel cell cold-start operation.

NOMENCLATURE

D	diameter of molecule, m
k	thermal conductivity, W/m K
P	pressure, Pa
R	universal gas constant, 8.134 J/mol K
S	source term
t	time, s
T	temperature, K
$\vec{u}$	velocity vector, m/s

Greeks

ρ	density, kg m^{-3}
Φ	phase potential, V
λ	membrane water content
ε	porosity
η	surface overpotential, V
$\vec{\tau}$	shear stress, N m^{-2}
δ	thickness, m
σ	ionic conductivity, S m^{-1};

Superscripts and Subscripts

eff	effective value
g	gas phase
m	mass

Mathematical modeling and analysis

Figure 1 schematically shows the components of a PEFC and the involved electrochemical reactions. A typical PEFC consists of bipolar plate, gas diffusion layer (GDL), catalyst layer (CL), and proton conducting membrane. The geometrical and physical parameters of these components are summarized in Table 1. At the electrochemical reaction surface in the cathode CL, oxygen reacts with protons and electrons from the hydrogen dissociation in the anode (see Fig. 1). Water and heat are byproducts of the oxygen reduction reaction (ORR).

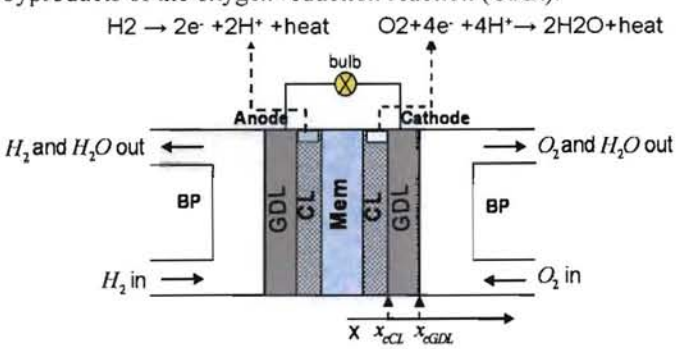

Figure 1. Schematic of a PEFC.

At the subzero condition, the oxygen reduction reaction (ORR) is still active and able to produce water. Water production under subfreezing conditions has been observed directly by neutron images as shown in Fig. 2, which display the evolution of the average water content under the channel and land, respectively. The neutron imaging was conducted at the NIST Center for Neutron Research (NCNR) on the thermal beam tube 2. The measurements were conducted using beam #1 and aperture #4 with a fluence rate of 2×107 neutrons/(cm^2 s). The fuel cell was operated at subfreezing temperature of -20 °C, therefore the water will likely exist in solid state. The water content increases steadily with time due to the water production by the ORR. At subfreezing temperatures, water freezes in the pores of the catalyst layer blocking the open pores required for reactant diffusion.

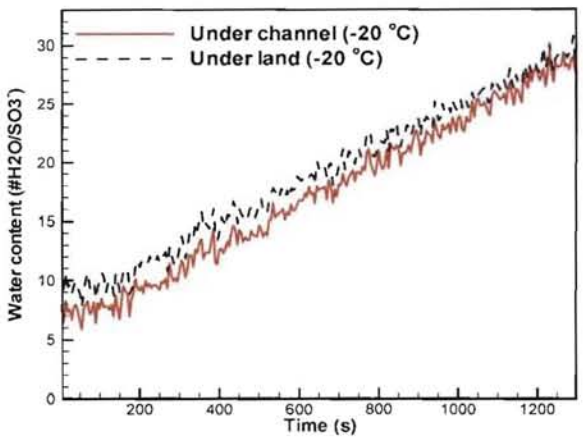

Fig. 2 The water content evolution from neutron images during fuel cell operation at subfreezing temperature -20 °C.

For single-layer electrodes or homogenous electrodes, the spatial variation of the reaction rate across the catalyst layer is almost uniform at small $\hbar$ s ($\hbar = \dfrac{\Delta U}{2\dfrac{RT}{\alpha_c F}}$) [16,17] (see Fig. 3), which is satisfied for most cold-start operation. During cold start, the reaction rate in the cathode can be expressed as [9]:

$$j = -a_0 i_{0,c}^{ref} (1 - s_{ice})^{r_a} \exp\left[-\frac{E_a}{R}\left(\frac{1}{T} - \frac{1}{353.15}\right)\right] \frac{C^{O2}}{C^{O2,ref}} \exp\left(-\frac{\alpha_c F}{RT} \cdot \eta\right) \quad (1)$$

In Eq. (1), α_c is the cathode transfer coefficient and its value can be a function of temperature. The surface overpotential is defined as:

$$\eta = \Phi_s - \Phi_e - U_o \quad (2)$$

Φ_s and Φ_e are electronic and electrolyte phase potentials, respectively. Typically due to the high electronic conductivity, Φ_s remains constant in the cathode, while Φ_e usually varies spatially due to the ionic resistance.

Eq. (1) directly shows that the reaction rate is a function of the local ice volume fraction as well as the local oxygen concentration. Both local ice volume fraction and oxygen concentration may vary spatially due to the local reaction and oxygen and water transport within the cathode. Therefore, the local reaction rate variation requires solving the coupled oxygen and water transport equations and electrochemical kinetics Eq. (1). A simplified assumption is to consider constant reaction rate in the electrode leading to uniform ice formation. Note that this assumption treats the catalyst layer as a number of separated small reactors in the through-plane direction. The reactors are operated at the uniform reaction rate, allowing the surface overpotentials to vary according to the local oxygen content and ice volume fraction. This treatment greatly simplifies the model and enables the impact of ice on electrode performance to be evaluated through temporal and spatial variations of the surface overpotential. We refer to this analysis as the pseudo-1D analysis. The uniform local transfer current and oxygen consumption rate can be expressed as:

$$j = -\frac{I}{\delta_{CL}} \text{ and } S_{O2} = -\frac{I}{4F\delta_{CL}} \tag{3}$$

Oxygen transport through the catalyst layer can be described by the species transport equation expressed in a 1D form as follow [9]:

$$\frac{\partial \varepsilon C^{O2}}{\partial t} + \frac{\partial u C^{O2}}{\partial x} = \frac{\partial}{\partial x}\left[D^{O2,eff} \frac{\partial C^{O2}}{\partial x} \right] + S^{O2} \tag{4}$$

Following the analysis of Ref. [9], the oxygen profile can be calculated by only considering the diffusive transport:

$$\frac{C^{O2}}{C^{O2}_{eCL}} = 1 - Da \frac{1-\bar{x}^2}{\varepsilon_{CL}^{\tau_d - \tau_{d,0}} [(1-s_{ice})]^{\tau_d}} \text{ where } \bar{x} = 1 - \frac{x_{cCL} - x}{\delta_{CL}} \tag{5}$$

where $\bar{x}$ is the dimensionless distance from the interface between the membrane and catalyst layer, and the dimensionless parameter, Da, is called the Damköhler number [9].

The oxygen profile in the catalyst layer of Eq. (5) can be substituted to Eq. (1), yielding [12]:

$$\eta(s_{ice}, T, \bar{x}) = -\frac{RT}{\alpha_c F} \ln\left(\frac{IC^{O2,ref}}{a_0 i_{0,c}^{ref} \exp\left[-\frac{E_a}{R}\left(\frac{1}{T_o} - \frac{1}{353.15} \right) \right] C^{O2}_{eCL} \delta_{CL}} \right)$$
$$- \frac{TE_a}{\alpha_c F}\left(\frac{1}{T} - \frac{1}{T_o} \right) + \frac{RT\tau_a}{\alpha_c F} \ln(1 - s_{ice}) + \frac{RT}{\alpha_c F} \ln\left(1 - Da \frac{1-\bar{x}^2}{\varepsilon_{CL}^{\tau_d - \tau_{d,0}} (1-s_{ice})^{\tau_d}} \right) \tag{6}$$
$$= \eta_o + \Delta\eta_T + \Delta\eta_{c,1} + \Delta\eta_{c,2}$$

where

$$\eta_o = -\frac{RT}{\alpha_c F} \ln\left(\frac{IC^{O2,ref}}{a_0 i_{0,c}^{ref} \exp\left[-\frac{E_a}{R}\left(\frac{1}{T_o} - \frac{1}{353.15} \right) \right] C^{O2}_{eCL} \delta_{CL}} \right),$$

$$\Delta\eta_T = -\frac{TE_a}{\alpha_c F}\left(\frac{1}{T} - \frac{1}{T_o} \right),\ \Delta\eta_{c,1} = \frac{RT\tau_a}{\alpha_c F} \ln(1 - s_{ice}) \text{ and}$$

$$\Delta\eta_{c,2} = \frac{RT}{\alpha_c F} \ln\left(1 - Da \frac{1-\bar{x}^2}{\varepsilon_{CL}^{\tau_d - \tau_{d,0}} (1-s_{ice})^{\tau_d}} \right)$$

Table 1. Geometrical and operating parameters.

Quantity	Value
Gas channel depth/width	0.5/1.0 mm
Shoulder width of the fuel cell	1.0 mm
GDL/Catalyst layer/Membrane thickness	0.2/0.01/0.03 mm
Anode/cathode pressures, P	2.0/2.0 atm
Activation energy for oxygen reduction reaction, E_a	73269 J/mol
Volume fraction of ionomer in catalyst layers, ε_m	0.2
O_2 diffusivity in cathode gas at standard condition, $D^{O2}_{M,0}$	3.24×10^{-5} m^2/s
Porosity of GDLs/catalyst layers ε	0.6/0.4

Results and Discussion

Figure 3 shows the profiles of dimensionless oxygen concentration within the cathode catalyst layer. The oxygen concentration decreases when approaching the membrane due to the oxygen reduction reaction. The oxygen concentration variation is small in most cases, even at s_{ice}=98%, about 5% drop is indicated (using $\tau_d = 1.5$). However, the oxygen profile is sensitive to the tortuosity of the catalyst layer. Mukherjee et al. [18] estimated the tortuosity from reconstructed CL microstructures between 2.5 and 3.0. At CL tortuosity, $\tau_d = 2.5$, a considerable drop of oxygen concentration is present at s_{ice}=96%. As the oxygen concentration affects the mass transport polarization, the associated cell voltage loss becomes important only at high s_{ice}.

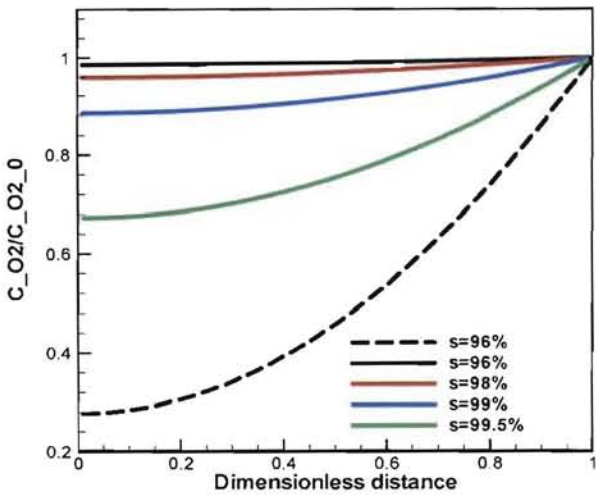

Fig. 3 The oxygen profiles within the cathode catalyst layer at different ice volume fractions. The dashed line is for the tortuosity of 2.5; while the rest are for 1.5.

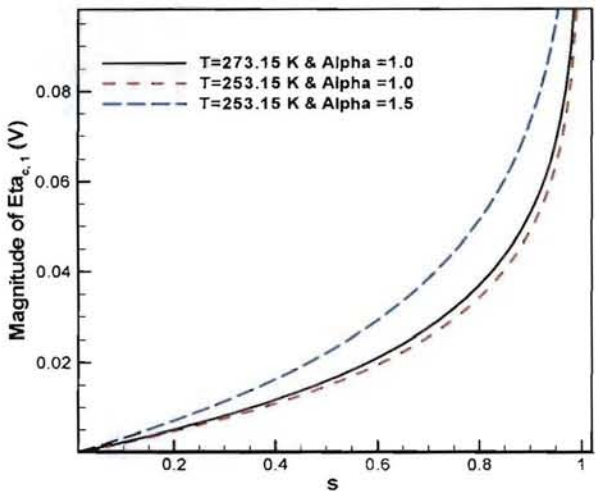

Figure 4. Profile of the $\Delta\eta_{c,l}$ as a function of the ice volume fraction.

Figure 4 presents the magnitude of $\Delta\eta_{c,l}$ as a function of the ice volume fraction. $\Delta\eta_{c,l}$ characterizes the impact of the ice coverage over the electrochemical reaction surface, and increases in magnitude quickly with s_{ice} as shown in Figure 4. Note that the ice coverage just temporarily blocks the oxygen access to the active reaction site, while the disabled interface, still accessible to electrons and protons, is generally able to recover after the solid water is removed. The figure shows that temperature has little impact on the value of $\Delta\eta_{c,l}$, instead the influence of the coefficient τ_α is evident. Further, based on previous analysis of Eq. 6, one can estimate the magnitudes of $\Delta\eta_T^{\max}$. Two values of the activation energy are considered [19], which render the magnitudes of $\Delta\eta_T^{\max}$ ~0.06 V and 0.025 V for Ea=73 and 28 KJ/mol, respectively, at cold-start temperature of 253.15 K. Note that the values of $\Delta\eta_T^{\max}$ exclude the temperature-difference of the Tafel slope. Therefore the value primarily gives the magnitude of the overpotential change due to the temperature-dependence of exchange current density. From this figure, it can be seen that $\Delta\eta_{c,l}$ is comparable with $\Delta\eta_T$ at low and intermediate ice volume fraction regions, while $\Delta\eta_{c,l}$ dominates at the high fraction of s_{ice}. At s_{ice}>95%, the adverse impact of the solid water will lead to a fast drop of the cell voltage.

During cold start, the cell temperature will increase from a subfreezing temperature to the optimal one. Temperature can affect the ionic conductivity and therefore the ohmic voltage loss ($\Delta V_{ohm} = R_\Omega I$). The ohimic resistance due to proton transport R_Ω^{H+} can be expressed by [9]:

$$R_\Omega^{H+} = \frac{\delta_m}{\sigma_m} + \frac{\delta_{aCL}}{2\sigma_m^{aCL,eff}} + \frac{\delta_{cCL}}{2\sigma_m^{cCL,eff}} \tag{7}$$

The above ionic conductivities σ_m, $\sigma_m^{aCL,eff}$, and $\sigma_m^{cCL,eff}$ are the averages over the membrane, anode and cathode catalyst layers, respectively. The latter two can be calculated by considering the Bruggeman correlation:

$$\sigma_m^{aCL,eff} = \varepsilon_m^{1.5}\sigma_m^{aCL} \text{ and } \sigma_m^{cCL,eff} = \varepsilon_m^{1.5}\sigma_m^{cCL} \tag{8}$$

The ionic conductivity σ_m is a function of the local water content and temperature, as indicated by Springer et al. [20] for standard (above-zero) operating condition. At subfreezing temperature, part of the water in the membrane may freeze and affect the ionic conductivity. Our previous study [12] measured the ionic conductivity of Nafion® 117 from -30 to 0 °C. The fitted ionic conductivity expression is as follow [12], also shown in Fig. 5:

$$\begin{aligned}
\sigma_m &= (0.01862\lambda - 0.02854)\exp\left[4029\left(\frac{1}{303}-\frac{1}{T}\right)\right] \\
&= (0.004320\lambda - 0.006620)\exp\left[4029\left(\frac{1}{273}-\frac{1}{T}\right)\right] \qquad \text{for } \lambda \le 7.22 \\
&= \sigma_{m,0}(\lambda)\exp\left[4029\left(\frac{1}{273}-\frac{1}{T}\right)\right] \\
\sigma_m &= \sigma_m(\lambda = 7.22) \qquad \text{for } \lambda > 7.22
\end{aligned} \tag{9}$$

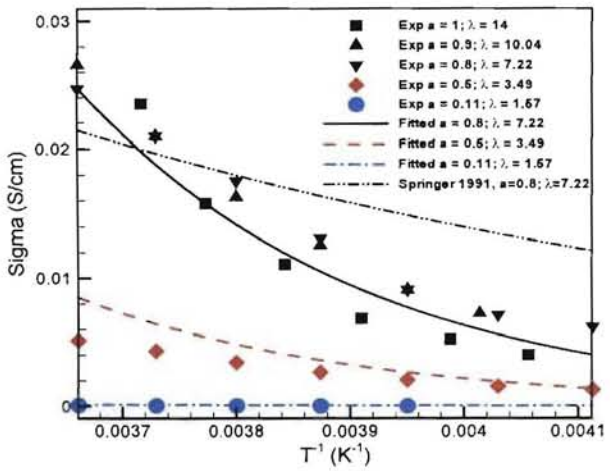

Figure 5. Dependence of the ionic conductivity on temperature and water content, and comparison of the fitting curve of Eq. (9) and experimental data based on the Nafion® 117 [12].

It can be seen that the ionic conductivity above λ >7.22 (the water activity, a>80%) shows a complex pattern of the water content dependence, which may due to the fact that part of water in the ionomer phase freezes. Note that a higher water content may reduce the portion of nonfreezing water through interacting with the sulfonic groups. For modeling/simulation purposes, Eq. (9) assumes the ionic conductivity is independent of λ for λ >7.22. Therefore, the change of cell voltage due to the ohmic resistance can be expressed by:

$$\Delta V_{ohm}^{H+} = R_{\Omega}^{H+} I$$
$$= \left(\frac{\delta_m}{\sigma_{m,0}(\lambda^m)} + \frac{\delta_{aCL}}{2\sigma_{m,0}(\lambda^{aCL})\varepsilon_m^{1.5}} + \frac{\delta_{cCL}}{2\sigma_{m,0}(\lambda^{cCL})\varepsilon_m^{1.5}} \right) \exp\left[-4029\left(\frac{1}{273} - \frac{1}{T} \right) \right] I$$
$$= R_{\Omega,273K}^{H+}(\bar{\lambda}) \exp\left[-4029\left(\frac{1}{273} - \frac{1}{T} \right) \right] I \quad (10)$$

Where $\bar{\lambda}$ is average over the whole MEA. To assess the temperature impact, one can differentiate the above equation and consider a temperature change of dT:

$$d(\Delta V_{ohm}^{H+}) = \left[\begin{array}{l} \dfrac{dR_{\Omega,273K}^{H+}}{d\lambda} \exp\left[-4029\left(\dfrac{1}{273} - \dfrac{1}{T} \right) \right] d\lambda \\ -\dfrac{4029}{T^2} R_{\Omega,273K}^{H+} \exp\left[-4029\left(\dfrac{1}{273} - \dfrac{1}{T} \right) \right] dT \end{array} \right] I \quad (11)$$

Note that if the hydration level of the MEA is always above 7.22, the first term in the bracket is zero. The second one can be used to estimate the magnitude of the ohmic-loss variation by integrating from T to T+dT. Considering λ =14, T=-30 °C and dT =30 °C as well as other parameters in Table 1, the value of $R_{\Omega,273K}^{H+}$ is ~700 mΩ cm^2, which renders $d(\Delta V_{ohm}^{H+})\Big|_{-30^\circ C}^{0^\circ C}$ ~0.18 V @ 0.1 A/cm^2. In addition, using the data of Springer et al. [20], the value of $d(\Delta V_{ohm}^{H+})\Big|_{-30^\circ C}^{0^\circ C}$ ~0.03V, which underestimates the degree of temperature dependence of the Ohmic polarization during cold start.

Conclusion

This paper presents a theoretical study on the electrochemical and transport processes within the cathode catalyst layer of PEFC during cold-start. Theoretical analysis was developed and spatial variations of the oxygen concentration and overpotential were investigated. Oxygen transport limitation was found to occur at high ice volume fraction regions, especially in CL with high tortuosities. We found that the overpotential change due to the temperature-dependent reaction kinetics is around 0.02-0.06 V at the cold-start temperature of 253.15 K and the voltage variation due to the temperature-dependent Ohmic loss ~0.18 V based on the new experimental data for the membrane ionic conductivity at subfreezing temperature.

ACKNOWLEDGMENTS

Partial support of this work by the Academic Senate Council on Research, Computing & Library Resources is gratefully acknowledged. LANL acknowledges funding provided by the U.S. Department of Energy, Fuel Cell Technologies Program.

REFERENCES

1. J. Larminie & A. Dicks, Fuel Cell Systems Explained (2nd Edition), John Wiley & Sons 2003.
2. Y. Hishinuma, T. Chikahisa, F. Kagami, and T. Ogawa, *JSME Int. J., Ser. B,* 47, 235 (2004).
3. M. S. Wilson, J. A. Valerio, S. Gottesfeld, *Electrochim. Acta*, 40, 1995, 355.
4. R. C. McDonald, C. K. Mittelsteadt, and E. L. Thompson, *Fuel Cells*, 4, 2004, 208.
5. E. Cho, J. J. Ko, H. Y. Ha, S. A. Hong, K. Y. Lee, T. W. Lim, and I. H. Oh, *J. Electrochem. Soc.*, 151, 2004, A661.
6. M. Oszcipok, D. Riemann, U. Kronenwett, M. Kreideweis, and M. Zedda, *J. Power Sources*, 145, 2005, 407.
7. Q. Yana, H. Toghianib, Y-W. Leea, K. Liangb and H. Causey, *J. Power Sources*, 160, 2006, 1242.
8. R. Mukundan, Y. S. Kim, T. Rockward , J. R. Davey, B. S. Pivovar, D. S. Hussey, D. L. Jacobson, M. Arif, and R. L. Borup, *ECS Transactions*, 11, 2007, 543-552.
9. Y. Wang, J. Electrochem. Soc., 154, 2007, B1041-B1048.
10. J. Chen and Y. Wang, "Analysis of Subzero Start-Up for Polymer Electrolyte Fuel Cells", ECS Trans. 13 (11), 13 (2008).
11. Y. Wang, Jeff Mishler, Partha Mukherjee, Rangachary Mukundan, and Rodney Borup, Pseudo One-

Dimensional Analysis of Polymer Electrolyte Fuel Cell Cold-Start, ECS Transactions, 25(1), 2009, 285 - 294.
12. Yun Wang, Partha P. Mukherjee, Jeff Mishler, Rangachary Mukundan, and Rodney L. Borup , "Cold Start of Polymer Electrolyte Fuel Cells: Three-Stage Startup Characterization", Electrochimica Acta, in press.
13. L. Mao and C.Y. Wang, *J. Electrochem. Soc.* 154, 2007, B341.
14. H. Meng, Int. J. Hydrogen Energy, 33, 2008, 5738-5747.
15. K. Jiao and X. Li, Electrochimica Acta 54 (27), (2009) 6876-6891.
16. Y. Wang and Xuhui Feng, J. Electrochem. Soc., 155(12), 2008, B1289-B1295.
17. Y. Wang and Xuhui Feng, J. Electrochem. Soc., 156(3) (2009) B403-B409.
18. P. P. Mukherjee and C. Y. Wang, J. Electrochem. Soc., 153, 2006, A840-849.
19. Parthasarathy, S. Srinivasan, and A. J. Appleby, J. Electrochem. Soc., 139, 1992, 2530.
20. T.E. Springer, T. A. Zawodinski, and S. Gottesfeld, J. Electrochem. Soc., 138, 1991, 2334–2341.